Comparison of the Marcus and Pekar partitions in the context of non-equilibrium, polarizable-continuum solvation models

Zhi-Qiang You,[1] Jan-Michael Mewes,[2] Andreas Dreuw,[2] and John M. Herbert[1,a)]
[1]*Department of Chemistry and Biochemistry, The Ohio State University, Columbus, Ohio 43210, USA*
[2]*Interdisciplinary Center for Scientific Computing, Ruprechts-Karls University, Im Neuenheimer Feld 368, 69120 Heidelberg, Germany*

(Received 4 September 2015; accepted 11 November 2015; published online 24 November 2015)

The Marcus and Pekar partitions are common, alternative models to describe the non-equilibrium dielectric polarization response that accompanies instantaneous perturbation of a solute embedded in a dielectric continuum. Examples of such a perturbation include vertical electronic excitation and vertical ionization of a solution-phase molecule. Here, we provide a general derivation of the accompanying polarization response, for a quantum-mechanical solute described within the framework of a polarizable continuum model (PCM) of electrostatic solvation. Although the non-equilibrium free energy is formally equivalent within the two partitions, albeit partitioned differently into "fast" versus "slow" polarization contributions, discretization of the PCM integral equations fails to preserve certain symmetries contained in these equations (except in the case of the conductor-like models or when the solute cavity is spherical), leading to alternative, non-equivalent matrix equations. Unlike the total equilibrium solvation energy, however, which can differ dramatically between different formulations, we demonstrate that the equivalence of the Marcus and Pekar partitions for the non-equilibrium solvation correction is preserved to high accuracy. Differences in vertical excitation and ionization energies are <0.2 eV (and often <0.01 eV), even for systems specifically selected to afford a large polarization response. Numerical results therefore support the interchangeability of the Marcus and Pekar partitions, but also caution against relying too much on the fast PCM charges for interpretive value, as these charges differ greatly between the two partitions, especially in polar solvents. [http://dx.doi.org/10.1063/1.4936357]

I. INTRODUCTION

Many important (bio)chemical processes involve excited electronic states in the condensed phase, which cry out for effective and reliable computational methods to reproduce solvation effects on excited states. Here, we are interested in quantum-mechanical continuum solvation models[1–4] in which the solvent is a structureless, homogeneous dielectric medium and electrostatic solvation effects are captured by means of a reaction-field operator that modifies the solute's Hamiltonian. We are specifically interested in "apparent surface charge" models,[1] which in quantum chemistry are most often known as polarizable continuum models (PCMs).[1,3,4] Amongst these, the most common are the conductor-like PCM (C-PCM),[5,6] which works well in high-dielectric solvents,[7] and the "integral equation formulation" (IEF-PCM),[8] which is a more formally sound treatment of electrostatics in low-dielectric solvents. IEF-PCM is also known as the "surface and simulation of volume polarization for electrostatics" [SS(V)PE] model,[9] which was developed independently.[10] Consult Refs. 4, 7, or 11 for a formal discussion of the connections between these models.

For "static" (equilibrium, ground-state) solvation, it has been established that PCMs are capable of providing free energies of solvation with an accuracy of a few kcal/mol for small- to medium-size molecules, although additional, non-electrostatic contributions to solvation must be included to achieve this level of accuracy.[12–15] (Non-electrostatic terms will not be considered here.) However, there is still a challenge to deal with dynamic events, e.g., vertical electronic transitions or vertical ionization. Within the PCM formalism, two different approaches have been developed for such cases. The linear response (LR) approach[16,17] is derived by adding the reaction-field operator into the LR Kohn-Sham equation that is solved in time-dependent density functional theory (TDDFT), resulting in an extra Coulomb term that is related to the response of the solvent to the TDDFT transition density. Alternatively, the state-specific (SS) method computes excited states as solutions of a nonlinear Schrödinger equation,[18–26] in which the reaction-field operator includes a term describing how the solute's excited-state electron density polarizes the continuum. It is similar to the reaction-field model for the ground state except that the reaction field includes the relaxation of electronic polarization of the solvent (represented in a continuum picture using the solvent's optical dielectric constant, ε_{opt}) with respect to the excited-state density of the specific excited state in question.

In vertical excitation or ionization, the solute undergoes an abrupt change in its charge distribution. Various microscopic motions of the solvent have characteristic times to reach certain polarization response. The fast part of the solvent response (electrons) can follow such a dynamic process while

a)herbert@chemistry.ohio-state.edu

the remaining degrees of freedom (nuclei) remain unchanged as in the initial state. It is this partition the solvent response that gives rise to non-equilibrium solvation.

In equilibrium, the solvent polarization $\boldsymbol{P}(\boldsymbol{r})$ is governed by the static electric susceptibility, $\chi_e = (\varepsilon - 1)/4\pi$:

$$\boldsymbol{P}(\boldsymbol{r}) = \chi_e \boldsymbol{E}(\boldsymbol{r}). \tag{1}$$

Here, ε is the static dielectric constant and $\boldsymbol{E}(\boldsymbol{r})$ is the electric field in the dielectric solvent. In a non-equilibrium situation, the total polarization $\boldsymbol{P}(\boldsymbol{r})$ is described as the sum of the fast and slow components,

$$\boldsymbol{P}(\boldsymbol{r}) = \boldsymbol{P}^{\text{fast}}(\boldsymbol{r}) + \boldsymbol{P}^{\text{slow}}(\boldsymbol{r}). \tag{2}$$

Two different partition schemes are common in the literature and are traditionally ascribed to Marcus[27,28] and to Pekar.[29]

In the Marcus partition (MP),[27,28,30,31] the fast component of the solvent polarization remains in equilibrium with the electric field arising from the solute charge distribution, and furthermore, the slow component of the polarization remains unchanged in the "early" (E) time. Thus, the fast solvent polarization in the "actual" (A) time is given by

$$\boldsymbol{P}_{\text{A}}^{\text{fast}} = \chi_{\text{fast}} \boldsymbol{E}(\rho_{\text{A}}^{\text{solute}}, \boldsymbol{P}_{\text{A}}^{\text{fast}}, \boldsymbol{P}_{\text{E}}^{\text{slow}}), \tag{3}$$

where $\chi_{\text{fast}} = (\varepsilon_{\text{fast}} - 1)/4\pi$ and $\varepsilon_{\text{fast}}$ is the dielectric constant associated with whatever part of the solvent polarization responds quickly enough to follow the perturbation. One can then separate the fast and slow solvent polarizations in equilibrium:

$$\boldsymbol{P}^{\text{fast}} = \chi_{\text{fast}} \boldsymbol{E}, \tag{4}$$

$$\boldsymbol{P}^{\text{slow}} = \chi_{\text{slow}} \boldsymbol{E} = \boldsymbol{P} - \boldsymbol{P}^{\text{fast}}. \tag{5}$$

Here, the static susceptibility χ_e has been separated into two parts, $\chi_e = \chi_{\text{fast}} + \chi_{\text{slow}}$, with

$$\chi_{\text{fast}} = (\varepsilon_{\text{fast}} - 1)/4\pi, \tag{6}$$

$$\chi_{\text{slow}} = (\varepsilon - \varepsilon_{\text{fast}})/4\pi. \tag{7}$$

This is consistent with the phenomenological theory of frequency-dependent dielectric polarization.[32]

In the Pekar partition (PP),[29,33] the fast polarization equilibrates without taking note of the effect from the "early" polarization, $\boldsymbol{P}^{\text{slow}}$:

$$\boldsymbol{P}_{\text{A}}^{\text{fast,PP}} = \chi_{\text{fast}} \boldsymbol{E}(\rho_{\text{A}}^{\text{solute}}, \boldsymbol{P}_{\text{A}}^{\text{fast,PP}}). \tag{8}$$

As such, the slow component of the solvent polarization in equilibrium is

$$\boldsymbol{P}^{\text{slow,PP}} = \boldsymbol{P} - \boldsymbol{P}^{\text{fast,PP}}. \tag{9}$$

Comparing Eqs. (4) and (8), we see that within the Marcus partition, the fast solvent polarization depends on both ε and $\varepsilon_{\text{fast}}$, but within the Pekar partition, it depends on $\varepsilon_{\text{fast}}$ alone. The quantity $\varepsilon_{\text{fast}}$ is often taken to be the "optical" dielectric constant, $\varepsilon_{\text{opt}} = n^2$, where n denotes the solvent's index of refraction. For most solvents, ε_{opt} lies in the range from 1.5 to 3.0.[34] For the Marcus partition, the ratio of the fast and slow polarization in the ground state is

$$\frac{\boldsymbol{P}^{\text{fast}}}{\boldsymbol{P}^{\text{slow}}} = \frac{\varepsilon_{\text{opt}} - 1}{\varepsilon - \varepsilon_{\text{opt}}}. \tag{10}$$

It follows that in highly polar solvents, where $\varepsilon \gg \varepsilon_{\text{opt}}$, there is something of an upper bound on the fast contribution to the ground-state solvent polarization contribution in the Pekar case, whereas in the Marcus case, the effect of fast polarization becomes negligible in the same limit. Only the latter result seems intuitively reasonable, as one expects that the nuclear (slow) polarization should be the overwhelming contribution to the electrostatics when $\varepsilon \gg \varepsilon_{\text{opt}}$. This counterintuitive feature of the Pekar partition has been pointed out previously.[30,35]

Although the two partitions have different physical descriptions for the fast and slow components of the solvent polarization, both the total polarization charge and the total electrostatic free energy for a non-equilibrium situation are equivalent between these two partitions, in the case of a linear dielectric medium and a classical Onsager solvation model consisting of a point dipole in a spherical cavity.[36] For a quantum-mechanical solvation model, Marenich *et al.*[37] showed that the solvent polarization charges within the PCM formalism are partition-independent, and thus, they suggest that the two partitions should yield identical values for the total non-equilibrium PCM polarization energy, in the case of a linear dielectric medium. [Recall that a "linear" dielectric is one for which $\boldsymbol{P} = \chi \boldsymbol{E}$, as for example in Eqs. (4) and (5).]

In the course of developing a general formalism for non-equilibrium SS-PCM calculations (building upon our recent work in Ref. 38, which was implicitly based on the Marcus partition), we discovered that the Marcus and Pekar partitions are *not* numerically equivalent, strictly speaking, for sophisticated PCMs such as IEF-PCM/SS(V)PE, although they are for C-PCM. The lack of equivalence in the former case is reminiscent of numerical differences between IEF-PCM and SS(V)PE, which are formally equivalent at the level of integral equations. These differences arise due to ambiguities in how to discretize the integral equations, a topic that has been investigated previously by one of us.[7] However, in contrast to the total PCM solvation energy, which can be quite sensitive to this issue, we find that differences between non-equilibrium vertical excitation and ionization energies are quite small, when comparing IEF-PCM to SS(V)PE and when comparing the Marcus partition to the Pekar partition.

In Section II, we review the SS method and provide a general derivation that is consistent with the PCM formalism, and which makes clear the relationship between non-equilibrium SS free energies in the Marcus and Pekar partitions. We also introduce a practical method for calculating vertical excitation energies and ionization energies within a non-equilibrium PCM framework. The test systems are introduced in Section III, and numerical results are the presented in Section IV.

II. THEORY

A. State-specific method for excited states

In the SS method, a generic solute excited state Ψ_i (in solution) is obtained as a solution of a nonlinear Schrödinger equation

$$\hat{H}_i^{\text{SS}} |\Psi_i\rangle = E_i^{\text{SS}} |\Psi_i\rangle. \tag{11}$$

This equation is nonlinear because the effective Hamiltonian

$$\hat{H}_k^{\mathrm{SS}} = \hat{H}^{\mathrm{vac}} + \hat{V}_0^{\mathrm{slow}} + \hat{V}_k^{\mathrm{fast}} \tag{12}$$

depends upon the solute's charge distribution, $\rho_k(\boldsymbol{r}) = |\Psi_k(\boldsymbol{r})|^2$, with $k = 0$ representing the ground state. Here, $\hat{H}^{\mathrm{vac}}$ is the usual Hamiltonian for the solute in vacuum and the reaction-field operator $\hat{V}_k$ generates the electrostatic potential of the apparent surface charge density, $\sigma_k(\boldsymbol{s})$. In the non-equilibrium case, there are two apparent surface charges, corresponding to slow and fast polarization response, hence, $\hat{V}_0^{\mathrm{slow}}$ and $\hat{V}_k^{\mathrm{fast}}$ in Eq. (12). How σ_0^{slow} and σ_k^{fast} are determined depends upon the particular flavor of PCM in question. The corresponding electrostatic potentials are

$$V_k(\boldsymbol{r}) = \int_{\boldsymbol{\Gamma}} d\boldsymbol{s}\, \frac{\sigma_k(\boldsymbol{s})}{|\boldsymbol{r}-\boldsymbol{s}|}, \tag{13}$$

where the integral runs over the cavity surface, $\boldsymbol{\Gamma}$.

The work to polarize the dielectric is a half of the electrostatic interaction between solute and solvent,[32,39]

$$W_k = \tfrac{1}{2}\langle\Psi_k|\hat{V}_k|\Psi_k\rangle = \tfrac{1}{2}\int_{\mathbf{V}} d\boldsymbol{r}\, \rho_k(\boldsymbol{r})\, V_k(\boldsymbol{r}). \tag{14}$$

Unlike Eq. (13), this is a volume integral over all space ($\mathbf{V}$). Alternatively, W_k can be expressed as

$$\begin{aligned} W_k &= \tfrac{1}{2}\int_{\mathbf{V}} d\boldsymbol{r}\, \rho_k(\boldsymbol{r}) \int_{\boldsymbol{\Gamma}} d\boldsymbol{s}\, \frac{\sigma_k(\boldsymbol{s})}{|\boldsymbol{r}-\boldsymbol{s}|} \\ &= \tfrac{1}{2}\int_{\boldsymbol{\Gamma}} d\boldsymbol{s}\, \sigma_k(\boldsymbol{s}) \int_{\mathbf{V}} d\boldsymbol{r}\, \frac{\rho_k(\boldsymbol{r})}{|\boldsymbol{s}-\boldsymbol{r}|} \\ &= \tfrac{1}{2}\int_{\boldsymbol{\Gamma}} d\boldsymbol{s}\, \sigma_k(\boldsymbol{s})\, \phi^{\rho_k}(\boldsymbol{s}). \end{aligned} \tag{15}$$

Here, we introduce the notation $\phi^{\rho}(\boldsymbol{s})$ to indicate the electrostatic potential on the cavity surface that is generated by the density $\rho(\boldsymbol{r})$. In the specific case of Eq. (15), this density is $\rho_k = |\Psi_k|^2$.

Having determined the excited-state energy E_i^{SS} from Eq. (11), the non-equilibrium electrostatic *free* energy for state Ψ_i is

$$G_i^{\mathrm{SS}} = E_i^{\mathrm{SS}} - W_0^{\mathrm{slow}} - W_i^{\mathrm{fast}} + W_{0,i}. \tag{16}$$

The final term, which arises only in the Marcus partition, represents the Coulomb interaction between the fast and slow polarization charges and describes a physical situation in which the fast polarization is affected by "earlier," equilibrium slow components.[19,27,40] Specifically,[1,41]

$$W_{0,i} = \tfrac{1}{2}\int_{\boldsymbol{\Gamma}} d\boldsymbol{s}\, \phi^{\sigma_0^{\mathrm{slow}}}(\boldsymbol{s})\left[\sigma_i^{\mathrm{fast}}(\boldsymbol{s}) - \sigma_0^{\mathrm{fast}}(\boldsymbol{s})\right], \tag{17}$$

where $\phi^{\sigma_0^{\mathrm{slow}}}(\boldsymbol{s})$ is the slow surface charge potential generated by the ground-state solvent polarization:

$$\phi^{\sigma}(\boldsymbol{s}) = \hat{S}\sigma(\boldsymbol{s}) = \int_{\boldsymbol{\Gamma}} d\boldsymbol{s}'\, \frac{\sigma(\boldsymbol{s}')}{|\boldsymbol{s}-\boldsymbol{s}'|}. \tag{18}$$

The operator $\hat{S}$, which is defined by the second equality in Eq. (18), generates the electrostatic potential for a given surface charge distribution.[4,11] Finally, the state-specific vertical excitation energy is defined as the difference between the SS free energy of state i in Eq. (16) and the equilibrium ground-state free energy, G_0. This excitation energy is

$$\begin{aligned} \omega_i^{\mathrm{SS}} &= G_i^{\mathrm{SS}} - G_0 \\ &= (E_i^{\mathrm{SS}} - W_0^{\mathrm{slow}} - W_i^{\mathrm{fast}} + W_{0,i}) \\ &\quad - (E_0 - W_0^{\mathrm{fast}} - W_0^{\mathrm{slow}} + W_{0,0}) \\ &= \Delta E_{i0}^{\mathrm{SS}} - W_i^{\mathrm{fast}} + W_0^{\mathrm{fast}} + W_{0,i}. \end{aligned} \tag{19}$$

The final equality follows by defining $\Delta E_{i0}^{\mathrm{SS}} = E_i^{\mathrm{SS}} - E_0$ and by noting that $W_{0,0} = 0$ according to Eq. (17).

Within the quantum-mechanical framework, it is not trivial to obtain the eigenstate solution for Eq. (11). The solute is polarized self-consistently with respect to the solvent's reaction field. In case of vertical ionization (rather than excitation), both the ionized and non-ionized states can be treated within a ground-state formalism. For vertical excitations, self-consistent SS models have been developed for various excited-state methods, including both TDDFT and configuration interaction singles (CIS).[21,37]

B. Partition dependence of the state-specific excitation energy and free energy

In this section, examine how the SS electrostatic free energy and the corresponding excitation energy depend upon the choice of Marcus versus Pekar partition, within the PCM formalism. We begin with a brief introduction to this formalism. In a linear dielectric material, the apparent surface charge density $\sigma(\boldsymbol{s})$ satisfies an equation that can be expressed generically as[4,11]

$$\hat{K}_{\varepsilon}\,\sigma(\boldsymbol{s}) = \hat{R}_{\varepsilon}\,\phi^{\rho}(\boldsymbol{s}). \tag{20}$$

The integral operators $\hat{K}_{\varepsilon}$ and $\hat{R}_{\varepsilon}$ depend upon the cavity surface definition ($\boldsymbol{\Gamma}$) and the dielectric constant and have different forms for different PCMs.[4,7,11] Use of the fast dielectric constant in Eq. (20) affords an equation for the surface charge σ^{fast} corresponding to the fast component of the solvent polarization for the state i,[35,36,41] but the electrostatic potential that appears on the right depends upon whether the Marcus or Pekar partition is employed:

$$\hat{K}_{\varepsilon_{\mathrm{fast}}}\sigma_i^{\mathrm{fast}}(\boldsymbol{s}) = \hat{R}_{\varepsilon_{\mathrm{fast}}}\begin{cases} \phi^{\rho_i}(\boldsymbol{s}) + \phi^{\sigma_0^{\mathrm{slow}}}(\boldsymbol{s}) & \text{(Marcus)} \\ \phi^{\rho_i}(\boldsymbol{s}) & \text{(Pekar)} \end{cases}. \tag{21}$$

The slow component of the ground-state solvent polarization is

$$\sigma_0^{\mathrm{slow}}(\boldsymbol{s}) = \begin{cases} \left(\chi_{\mathrm{slow}}/\chi_e\right)\sigma_0(\boldsymbol{s}) & \text{(Marcus)} \\ \sigma_0(\boldsymbol{s}) - \sigma_0^{\mathrm{fast}}(\boldsymbol{s}) & \text{(Pekar)} \end{cases}. \tag{22}$$

It has been shown that the total non-equilibrium apparent surface charge density is partition-independent[37] and is given by

$$\sigma_i(\boldsymbol{s}) = \hat{Q}_{\varepsilon_{\mathrm{fast}}}\phi^{\rho_i}(\boldsymbol{s}) + (\hat{Q}_{\varepsilon_0} - \hat{Q}_{\varepsilon_{\mathrm{fast}}})\phi^{\rho_0}(\boldsymbol{s}), \tag{23}$$

where $\hat{Q}_{\varepsilon} = \hat{K}_{\varepsilon}^{-1}\hat{R}_{\varepsilon}$ is the PCM solvent response operator for a generic dielectric constant ε. (We henceforth use ε_0 to denote the ground-state, static dielectric constant.) If ρ_i in Eq. (23) is determined self-consistently, then the reaction-field potentials are identical irrespective of which partition is

employed;[37] thus, the eigenvectors and eigenvalues in Eq. (11) are partition-independent as well.

However, this is *not* true in practical implementation for the SS free energy, nor is it true for the SS excitation energy; these may differ depending on the partition. To understand why, let us derive the free-energy difference between the partitions and then discuss discretization. We begin from the SS excitation energy in Eq. (19). Since the eigenvalues in Eq. (11) are partition-independent,[37] only the polarization energy terms need to be considered. For the Pekar partition, the polarization energy is given by

$$W_i^{\mathrm{PP}} = W_i^{\mathrm{fast}} - W_0^{\mathrm{fast}}. \tag{24}$$

Using Eqs. (15) and (21), we can express this as

$$\begin{aligned} W_i^{\mathrm{PP}} &= \tfrac{1}{2}\int_{\mathbf{\Gamma}} d\boldsymbol{s}\left[\phi^{\rho_i}(\boldsymbol{s})\,\sigma_i^{\mathrm{fast}}(\boldsymbol{s}) - \phi^{\rho_0}(\boldsymbol{s})\,\sigma_0^{\mathrm{fast}}(\boldsymbol{s})\right] \\ &= \tfrac{1}{2}\int_{\mathbf{\Gamma}} d\boldsymbol{s}\int_{\mathbf{\Gamma}} d\boldsymbol{s}'\,\phi^{\rho_i}(\boldsymbol{s})\,Q_{\varepsilon_{\mathrm{fast}}}(\boldsymbol{s},\boldsymbol{s}')\,\phi^{\rho_i}(\boldsymbol{s}') \\ &\quad - \tfrac{1}{2}\int_{\mathbf{\Gamma}} d\boldsymbol{s}\int_{\mathbf{\Gamma}} d\boldsymbol{s}'\,\phi^{\rho_0}(\boldsymbol{s})\,Q_{\varepsilon_{\mathrm{fast}}}(\boldsymbol{s},\boldsymbol{s}')\,\phi^{\rho_0}(\boldsymbol{s}'). \end{aligned} \tag{25}$$

Here, $Q(\boldsymbol{s},\boldsymbol{s}')$ is the kernel of the integral operator $\hat{Q} = \hat{K}^{-1}\hat{R}$, which acts on the surface electrostatic potential at the point $\boldsymbol{s}'$ to produce the induced surface charge at the point $\boldsymbol{s}$.

The polarization energy for the MP is

$$W_i^{\mathrm{MP}} = W_i^{\mathrm{fast}} - W_0^{\mathrm{fast}} - W_{0,i}, \tag{26}$$

or equivalently

$$W_i^{\mathrm{MP}} = W_i^{\mathrm{PP}} + \Delta W_i^{\mathrm{MP\text{-}PP}}, \tag{27}$$

where the difference, $\Delta W_i^{\mathrm{MP\text{-}PP}}$ is,

$$\begin{aligned} \Delta W_i^{\mathrm{MP\text{-}PP}} &= \tfrac{1}{2}\int_{\mathbf{\Gamma}} d\boldsymbol{s}\int_{\mathbf{\Gamma}} d\boldsymbol{s}'\,\phi^{\Delta\rho_i}(\boldsymbol{s})\,Q_{\varepsilon_{\mathrm{fast}}}(\boldsymbol{s},\boldsymbol{s}')\,\phi^{\sigma_0^{\mathrm{slow}}}(\boldsymbol{s}') \\ &\quad - \tfrac{1}{2}\int_{\mathbf{\Gamma}} d\boldsymbol{s}\int_{\mathbf{\Gamma}} d\boldsymbol{s}'\,\phi^{\sigma_0^{\mathrm{slow}}}(\boldsymbol{s})\,Q_{\varepsilon_{\mathrm{fast}}}(\boldsymbol{s},\boldsymbol{s}')\,\phi^{\Delta\rho_i}(\boldsymbol{s}'). \end{aligned} \tag{28}$$

We have defined $\Delta\rho_i = \rho_i - \rho_0$ as the difference density between excited state i and the ground state; this density generates an electrostatic potential $\phi^{\Delta\rho_i} = \phi^{\rho_i}(\boldsymbol{s}) - \phi^{\rho_0}(\boldsymbol{s})$. Note that $\phi^{\sigma_0^{\mathrm{slow}}}$ is determined by the Marcus scheme in Eq. (22).

To analyze Eq. (28), let us discretize it by introducing a finite grid over the cavity surface to convert Eq. (28) into an equation involving finite-dimensional vectors and matrices,

$$\Delta W_i^{\mathrm{MP\text{-}PP}} = \tfrac{1}{2}\mathbf{a}^\dagger\mathbf{Q}\mathbf{b} - \tfrac{1}{2}\mathbf{b}^\dagger\mathbf{Q}\mathbf{a}. \tag{29}$$

The column vectors $\mathbf{a}$ and $\mathbf{b}$ are discretized forms of the surface potentials $\phi^{\Delta\rho_i}$ and $\phi^{\sigma_0^{\mathrm{slow}}}$, respectively. Since the inner product $\mathbf{a}^\dagger\mathbf{Q}\mathbf{b}$ is real,

$$\begin{aligned} \Delta W_i^{\mathrm{MP\text{-}PP}} &= \tfrac{1}{2}(\mathbf{a}^\dagger\mathbf{Q}\mathbf{b})^\dagger - \tfrac{1}{2}\mathbf{b}^\dagger\mathbf{Q}\mathbf{a} \\ &= \tfrac{1}{2}\mathbf{b}^\dagger(\mathbf{Q}^\dagger - \mathbf{Q})\mathbf{a}. \end{aligned} \tag{30}$$

Formally speaking, the integral operator $\hat{Q}_\varepsilon = \hat{K}_\varepsilon^{-1}\hat{R}_\varepsilon$ is self-adjoint;[42] hence, $\Delta W_i^{\mathrm{MP\text{-}PP}}$ in Eq. (28) should vanish. Except in the case of a spherical cavity, however, discretization of this operator for the IEF-PCM/SS(V)PE approach does *not* afford a symmetric matrix $\mathbf{Q}_\varepsilon = \mathbf{K}_\varepsilon^{-1}\mathbf{R}_\varepsilon$, whereas the conductor-like (C-PCM) approach *does* afford a symmetric matrix, regardless of cavity shape.[43] As such, $\Delta W_i^{\mathrm{MP\text{-}PP}}$ vanishes (and thus, the partition dependence of the SS excitation energy vanishes) for C-PCM, but in practice, it does not for IEF-PCM/SS(V)PE. Since G_0 remains partition-independent even in the latter case, it must be that the SS electrostatic free energy, Eq. (16), is partition-*dependent* for IEF-PCM/SS(V)PE. The magnitude of this dependence is examined with numerical calculations in Sec. IV.

C. State-specific method for vertical ionization energies (VIEs)

A VIE is the difference between the ground-state energies of the neutral and ionized molecules, computed at the neutral molecule's geometry. In such a case, the ionized state is described using a ground-state, self-consistent reaction-field calculation, i.e., by solving Eq. (11). The lowest VIE in solvent is then calculated using Eq. (19), where ω_i^{SS} is understood to be the VIE rather than the vertical excitation energy in this case.

D. First-order approximation for vertical excitation energies

To obtain solutions of Eq. (11), one needs to consider the self-consistent polarization of the solute with respect to the solvent's reaction field. This requires *a priori* specification of the excited state of interest and may exhibit convergence problems, e.g., in the case of near degeneracies between states. In particular, the SS approach seems to be fundamentally ill-posed for describing solvent effects in the vicinity of a conical intersection, where relaxation of the solvent polarization using the upper state's wave function might change the ordering of the upper and lower states. Such problems have been encountered before by one of us,[44] in the context of excited-state QM/MM calculations involving polarizable force fields, and special techniques were developed in order to obtain sensible results. The SS nature of the correction also impacts formulas for oscillator strengths.[44]

The fundamental problem in these cases is that each wave function Ψ_i is an eigenfunction of a *different* Hamiltonian, since $\hat{H}_i^{\mathrm{SS}}$ in Eq. (11) depend upon the specific state of interest. To avoid such problems, we compute the vertical excitation energy using a first-order, perturbative approximation to the SS approach,[38,45–47] in what we have termed the "ptSS" method.[38] Consistent with conventional first-order perturbation theory, the wave functions $\Psi_i^{(0)}$ are used to compute the energy are eigenfunctions of a common, zeroth-order Hamiltonian. As such, they are mutually orthogonal and many problems can be avoided. One should note that the ptSS method is similar to the corrected linear response approach developed by Caricato *et al.*[47] The difference is that in corrected linear response, one solves TDDFT equations using the zeroth-order eigenstates as an initial guess, with inclusion of an explicit solvent contribution.

In the ptSS method,[38] we employ a Hamiltonian

$$\hat{H}_i^{\mathrm{ptSS}} = \hat{H}^{\mathrm{vac}} + \hat{V}_0^{\mathrm{slow}} + \hat{V}_0^{\mathrm{fast}} + \lambda\left(\hat{V}_i^{\mathrm{fast}} - \hat{V}_0^{\mathrm{fast}}\right), \tag{31}$$

in which λ is the usual perturbation parameter. The zeroth-order excited-state wavefunction, $\Psi_i^{(0)}$, is constructed using solvent-relaxed molecular orbitals obtained from a ground-state PCM calculation with the zeroth-order Hamiltonian $\hat{H}^{\text{vac}} + \hat{V}_0^{\text{slow}} + \hat{V}_0^{\text{fast}}$. The first-order correction to the energy of state i is

$$E_i^{(1)} = \langle \Psi_i^{(0)} | \hat{V}_{i^{(0)}}^{\text{fast}} - \hat{V}_0^{\text{fast}} | \Psi_i^{(0)} \rangle, \tag{32}$$

and the first-order polarization energy is

$$W_i^{(1)} = W_{i^{(0)}}^{\text{fast}} - W_0^{\text{fast}} - W_{0,i^{(0)}}. \tag{33}$$

The vertical excitation energy, corrected to first order for solvent effects, is then

$$\begin{aligned} \omega_i^{\text{ptSS,1st}} &= \left(G_i^{(0)} + G_i^{(1)}\right) - G_0 \\ &= \left(E_i^{(0)} - W_i^{(0)} + E_i^{(1)} - W_i^{(1)}\right) - \left(E_0 - W_0\right) \\ &= \Delta E_{i0}^{(0)} + E_i^{(1)} - W_i^{(1)}. \end{aligned} \tag{34}$$

We have simplified the final expression using the fact that $W_i^{(0)} = W_0$ because the same reaction field is used to compute both the ground state and the zeroth-order excited state.

The zeroth-order quantity $\Delta E_{i0}^{(0)}$ in Eq. (34) is partition-independent. The first-order energy $E_i^{(1)}$ can be shown to be partition-independent using Eqs. (15) and (21):

$$E_i^{(1)} = \int_\Gamma d\boldsymbol{s} \int_\Gamma d\boldsymbol{s}'\, \phi^{\rho_i^{(0)}}(\boldsymbol{s})\, Q_{\varepsilon_{\text{fast}}}(\boldsymbol{s},\boldsymbol{s}')\, \phi^{\Delta\rho_i^{(0)}}(\boldsymbol{s}'). \tag{35}$$

Finally, the first-order polarization energy, $W_i^{(1)}$, is nearly identical to the sum of the polarization energies in Eq. (19), except that Ψ_i is replaced with $\Psi_i^{(0)}$. This implies that $\omega_i^{\text{ptSS,1st}}$ inherits the partition-dependence of ω_i^{SS}.

The ptSS method has been implemented for various density-based[47] and wave function-based[38,48] excited-state methods. Despite the first-order nature of the correction, this approach does take into account the relaxation of the solvent's electronic degrees of freedom in response to excitation of the solute.[45,46] Analysis of a four-level model, in which the solvent wavefunction can be considered explicitly, demonstrates that the electronic relaxation term represents the static electronic response of the solvent to the change in the solute's dipole moment between ground and excited states.[46] For response-type excited-state methods such as TDDFT, the zeroth-order state cannot provide "real" excited-state properties such as the dipole moment, due to its failure to satisfy the Hellman–Feynman theorem, and in principle, calculation of excited-state properties requires solution of coupled-perturbed equations to obtain a "relaxed" density.[49] Formally speaking, such methods therefore require relaxed densities in order to obtain the correct ptSS excitation energy.[38,47] On the other hand, in previous work in which the solute wave functions were described using the algebraic diagrammatic construction (ADC),[50] we obtain reasonable results using unrelaxed densities obtained from the intermediate state representation formalism,[38] which include significant orbital relaxation effects[51,52] that presumably account for the very good agreement with the experimental data.

The ptSS method has been suggested to neglect dynamical correlations between the solute and the solvent, which is identified as the frequency-dependent perturbation caused by the solute oscillating at its Bohr frequency.[45,46] It has further been suggested that this dynamic response can be recovered using the linear response method.[45] In our perturbative version of the linear-response method (ptLR, see also Ref. 38), the first-order correction to the excitation energy is given by

$$E_i^{(1),\text{LR}} = \langle \Psi_0 | \hat{V}_{i^{(0)}}^{\text{fast,dyn}} | \Psi_i^{(0)} \rangle, \tag{36}$$

which is capable of recovering part of the dynamical correlation.[46] The surface charge potential in this equation is given by

$$V_i^{\text{fast,dyn}}(\boldsymbol{r}) = \int_\Gamma d\boldsymbol{s}\, \frac{\delta\sigma_i^{\text{fast}}(\boldsymbol{s})}{|\boldsymbol{r} - \boldsymbol{s}|}, \tag{37}$$

where the fast part of the solvent polarization $\delta\sigma_i^{\text{fast}}(\boldsymbol{s})$ changes following the variation of the density, i.e., the transition density for the excitation. This quantity can be computed using Eq. (21),[20]

$$\hat{K}_{\varepsilon_{\text{fast}}}\, \delta\sigma_i^{\text{fast}}(\boldsymbol{s}) = \hat{R}_{\varepsilon_{\text{fast}}}\, \phi^{\delta\rho_i}(\boldsymbol{s}). \tag{38}$$

Numerical results point to the complementarity of the LR and SS methods; though for polar solvents or weak transitions, the SS method has certain advantages. For a weakly polar solute in a non-polar solvent, the LR method provides more accurate results.[21] Inspired by the results in Ref. 21, we recently implemented the ptSS and ptLR approaches for use with both the TDDFT and ADC methods and assessed the results against a set of experimental benchmarks.[38] Detailed investigation of the ptSS and ptLR contributions provided, a different perspective on the relation of ptSS and ptLR formalisms. In the present work, we use one of the molecules (nitrobenzene) from Ref. 38 to illustrate the LR contribution to the vertical excitation energy.

III. COMPUTATIONAL DETAILS

A. Systems considered

Because significant solvent shifts are often obtained for excited states possessing charge-transfer (CT) character, several such systems will be considered here (see Fig. 1). These include a dimer composed of ethylene and the methaniminium cation ($C_2H_4 \cdots CH_4N^+$) and another dimer consisting of ethylene and tetrafluoroethylene ($C_2H_4 \cdots C_2F_4$). In both cases, one can identify a purely intermolecular CT state for which a significant solvent shift is expected. Within the SS-PCM formalism, the significant change in dipole moment from ground to excited state generates a significant solvent shift that is absent in the LR-PCM treatment due to the vanishing transition moment between ground and CT state.[38,45,46]

We also investigate the twisted intramolecular charge-transfer (TICT) state of 4-(*N*,*N*-dimethylamino)benzonitrile (DMABN) in acetonitrile.[53–55] DMABN is a prototypical example of a molecule that exhibits a TICT state[53] in which the qualitative character of the S_1 state is highly dependent upon molecular geometry. In its ground-state geometry, DMABN is planar and S_1 has very little CT character, whereas S_2 has significant CT character. However, rotation of the amino group

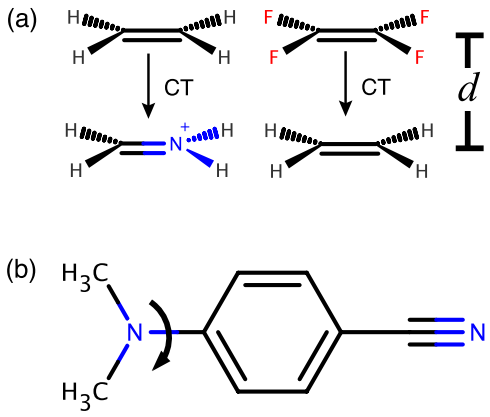

FIG. 1. Molecular structures considered in this work: (a) two CT dimer systems, $C_2H_4\cdots CH_4N^+$ and $C_2H_4\cdots C_2F_4$ and (b) the DMABN molecule, illustrating the twisting motion that causes the CT state to switch from S_2 at the ground-state geometry to S_1 at the TICT geometry.

by 90° [see Fig. 1(b)] reverses the order of the states: the CT state becomes S_1, and the "locally excited" (LE) state is pushed up to S_2. Since $Q(\boldsymbol{s},\boldsymbol{s}')$ depends on molecular geometry, via the cavity surface, we shall see that in the case of DMABN, the Marcus and Pekar partitions are not numerically equivalent even across the potential surface of the same molecule.

In order to make connection to our previous benchmark study,[38] wherein many of the molecules considered were nitrobenzene derivatives, we will also consider the 2 A_1 $\pi\pi^*$ excited state of nitrobenzene. This state is charactered by a HOMO − 1 to LUMO transition with significant CT character, yet enough oscillator strength to appear in the spectrum. Both LR- and SS-PCM are investigated in different solvents.

Finally, as an example of VIEs within the ptSS formalism, we examine aqueous phenol and phenolate in this capacity. The latter should engender much larger initial-state polarization, owing to its charge, whereas when computing the VIE of phenol, the charged species is the final state.

B. Theoretical methods

For the dimers, we used monomer geometries optimized in the gas phase (B3LYP/6-311+G*) and then placed at a face-to-face separation of $d = 3.5$ Å for $C_2H_4\cdots CH_4N^+$ and $d = 5.0$ Å for $C_2H_4\cdots C_2F_4$ (see Fig. 1). The planar ground state of DMABN and the solvent-relaxed geometry of nitrobenzene were optimized at the B3LYP/6-311G** level in combination with the C-PCM solvent model. The twisted geometry of DMABN was optimized in the S_1 state at the ωB97X/6-311G*/C-PCM level. Geometries of aqueous phenol and phenolate were taken from Ref. 56.

VIEs were computed using DFT and ptSS excitation energies using TDDFT. The basis sets employed were 6-311+G* (for $C_2H_4\cdots CH_4N^+$), cc-pVDZ (for $C_2H_4\cdots C_2F_4$ and nitrobenzene), 6-31G* (for DMBAN), and 6-31+G* (for phenol and phenolate). The long-range-corrected functional LRC-ωPBE,[57,58] with a non-empirically tuned range-separation parameter,[59] was used in all excitation energy calculations. This approach has been shown to yield reasonable CT excitation energies,[60,61] although the "optimal" (tuned) value for the range-separation parameter varies depending on the functional, basis set, and molecular system. Here, we tune this parameter as suggested in Ref. 60, by minimizing the sum of two absolute values: the difference between the highest occupied Kohn-Sham orbital energy and the ionization potential, and the difference between the lowest unoccupied Kohn-Sham orbital and the electron affinity.

We tested the C-PCM, IEF-PCM, and SS(V)PE solvation models. The IEF-PCM and SS(V)PE models are equivalent at the level of integral equations[9] but differ when the operator $\hat{K}$ in Eq. (20) is discretized to obtain a finite-dimensional matrix, $\mathbf{K}$.[4,7] Consistent with nomenclature in the literature,[7,8,11,62] we use "IEF-PCM" to mean the asymmetric choice $\mathbf{K} = \mathbf{DAS}$ (in the notation of Ref. 7), whereas "SS(V)PE" is taken to imply the symmetrized matrix $\mathbf{K} = (\mathbf{DAS} + \mathbf{SAD}^\dagger)/2$. Details of these models, written in a notation consistent with that used here, can be found in Refs. 4, 7, and 11. In all of the calculations presented here, we use the smooth "switching/Gaussian" (SWIG) discretization and cavity-construction algorithm of Ref. 43. All calculations were performed using a locally modified version of Q-Chem.[63] The non-equilibrium PCM approach for TD-DFT is available in Q-Chem v. 4.3 and the implementation for ADC(2), which we reported recently,[38] will be available in a future release of Q-Chem.

IV. RESULTS AND DISCUSSION

A. Discretization of the PCM matrices

The basic PCM working equation is a discretized form of Eq. (20):

$$\mathbf{K}_\varepsilon \mathbf{q} = \mathbf{R}_\varepsilon \mathbf{v} \tag{39}$$

with

$$\mathbf{R}_\varepsilon = -f_\varepsilon \left(\mathbf{I} - \frac{1}{2\pi}\mathbf{DA} \right). \tag{40}$$

Here, $f_\varepsilon = (\varepsilon - 1)/(\varepsilon + 1)$ and $\mathbf{A}$ is a diagonal matrix whose non-zero entries are the surface areas associated with the discretization points. (These areas, in turn, are related to the Lebedev integration weights for the surface grid points.[43,64]) Following the notation used in Ref. 7, the matrix $\mathbf{K}_\varepsilon$ is expressed as

$$\mathbf{K}_\varepsilon = \mathbf{S} - \frac{f_\varepsilon}{2\pi}\mathbf{X}, \tag{41}$$

and the choice

$$\mathbf{X} = \begin{cases} \mathbf{DAS} & \text{for IEF-PCM} \\ (\mathbf{DAS} + \mathbf{SAD}^\dagger)/2 & \text{for SS(V)PE} \end{cases} \tag{42}$$

defines the two solvation models considered here. The matrices $\mathbf{S}$ and $\mathbf{D}$ represent the surface-Coulomb operator and surface-dipole operator, respectively, and are fully defined in Ref. 11. Discretization preserves the symmetry of $\hat{S}$ (i.e., $\mathbf{S}^\dagger = \mathbf{S}$), but except for a spherical solute cavity, it does not preserve the identity $\hat{D}\hat{S} = \hat{S}\hat{D}^\dagger$. In other words, $\mathbf{DAS} \neq \mathbf{SAD}^\dagger$.[7]

Calculations for histidine using three variants of $\mathbf{X}$ were previously reported in Ref. 7, and a more complete set of

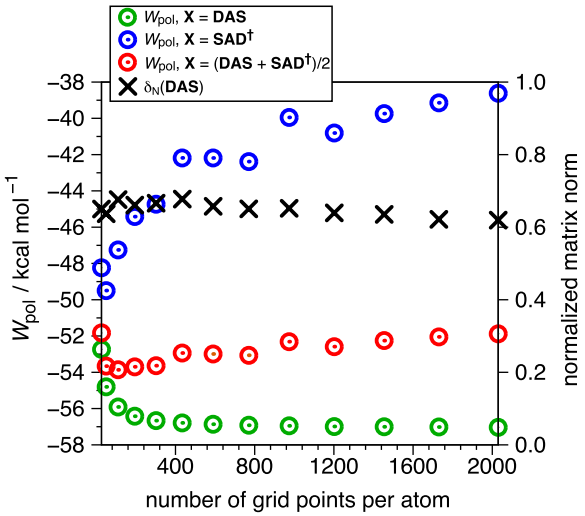

FIG. 2. Convergence of the polarization energy (axis at left), as a function of the number of Lebedev grid points per atomic sphere, for histidine described using the Amber99 force field. Results for three alternative choices for the matrix **X** in Eq. (41) are shown, along with the normalized norm of the matrix **DAS** – **SAD**† (axis at right).

calculations using denser grids is shown in Fig. 2. As observed in Ref. 7, the polarization energy

$$W_{\text{pol}} = \tfrac{1}{2}\mathbf{q}^\dagger\mathbf{v} = \tfrac{1}{2}\mathbf{v}^\dagger\mathbf{Q}_{\varepsilon_0}\mathbf{v} \tag{43}$$

converges smoothly as a function of number of grid points only for the IEF-PCM choice, **X** = **DAS**. For **X** = **SAD**†, W_{pol} does not converge for any reasonable grid density, and this significantly slows the convergence of the polarization energy for the SS(V)PE choice **X** = (**DAS** + **SAD**†)/2.

The difference between these two formulations can be measured in terms of the norm of the matrix **DAS** – **SAD**†, although the magnitude of this norm changes as a function of system and grid density. A better measure is what we will call the "normalized norm," which we define for a matrix **M** according to

$$\delta_{\text{N}}(\mathbf{M}) = \frac{\|\mathbf{M} - \mathbf{M}^\dagger\|}{\|\mathbf{M}\|}, \tag{44}$$

where $\|\mathbf{M}\| = (\sum_{i,j} M_{i,j}^2)^{1/2}$ indicates the usual Euclidean matrix norm. Figure 2 also provides a plot of δ_{N}(**DAS**) and we find that this measure of matrix asymmetry does not converge to zero, but instead hovers around 0.6 even for very dense integration grids. It is worth noting that the smooth SWIG discretization scheme[43] that we use here is not the cause of these issues. Consistent with previous results for equilibrium solvation,[7] we find that the SWIG procedure actually *reduces* discrepancies between the **X** = **DAS** and **X** = **SAD**† versions of the method. (Results using a primitive Lebedev discretization of the cavity surface, without the Gaussian blurring or switching function that characterize the SWIG discretization procedure, can be found in the supplementary material.[65])

It might be questioned whether discrepancies between IEF-PCM and SS(V)PE, and the slow convergence of the latter with respect to the discretization grid, might be artifacts of an inexact implementation of one or both models. In particular, our SWIG discretization procedure does not use the traditional definition of the diagonal matrix elements of **D**,[66] which is

$$D_{ii} = -\frac{1}{A_{ii}}\left(2\pi + \sum_{j\neq i} D_{ij}A_{jj}\right), \tag{45}$$

but rather[43]

$$D_{ii} = -\frac{S_{ii}}{2R_I} \qquad (\forall\, i \in I), \tag{46}$$

where R_I is the radius of the atomic sphere that contains the discretization point s_i. The traditional sum rule in Eq. (45) does not hold when a switching function allows discretization points to lie slightly above or below the cavity surface, and its naïve application in the context of SWIG discretization can lead to a loss of negative-definiteness in the matrix **Q**, which in turn leads to a total energy that is no longer variational.[43] The alternative formula in Eq. (46) eliminates this problem[7,43] and is exact in the case of a spherical cavity.[67] [As such, Eq. (46) amounts to a locally spherical approximation.]

The formula in Eq. (46) is used for all calculations reported here, except that in Fig. 3, we report IEF-PCM and SS(V)PE polarization energies for histidine (as in Fig. 2) and for phenolate, using the sum rule in Eq. (45) to define D_{ii}. In most cases, use of the sum rule leads to much better agreement between IEF-PCM and SS(V)PE solvation energies than is observed in Fig. 2, as the sum rule tends to amplify the value

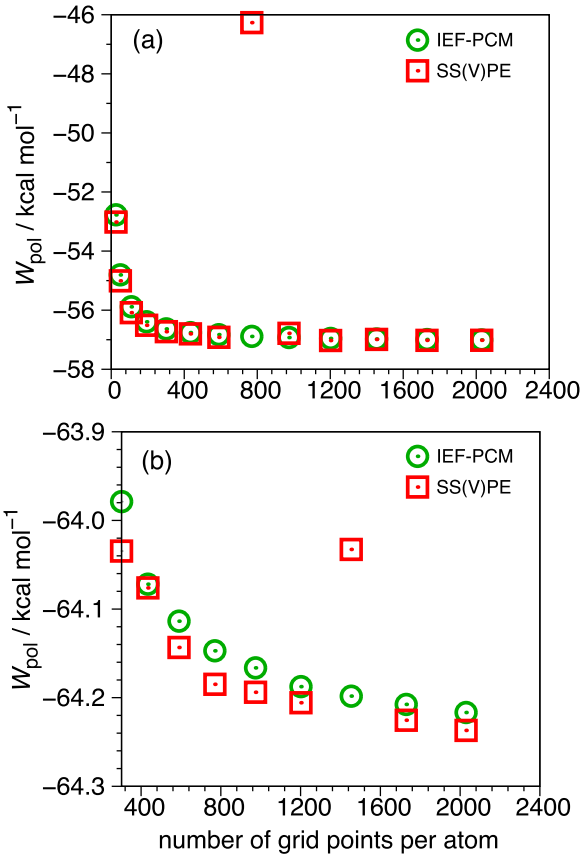

FIG. 3. Convergence of W_{pol} for (a) histidine at the Amber99 level and (b) phenolate at the LRC-ωPBE/6-31+G* level, when the sum rule in Eq. (45) is used to compute the diagonal matrix elements D_{ii}.

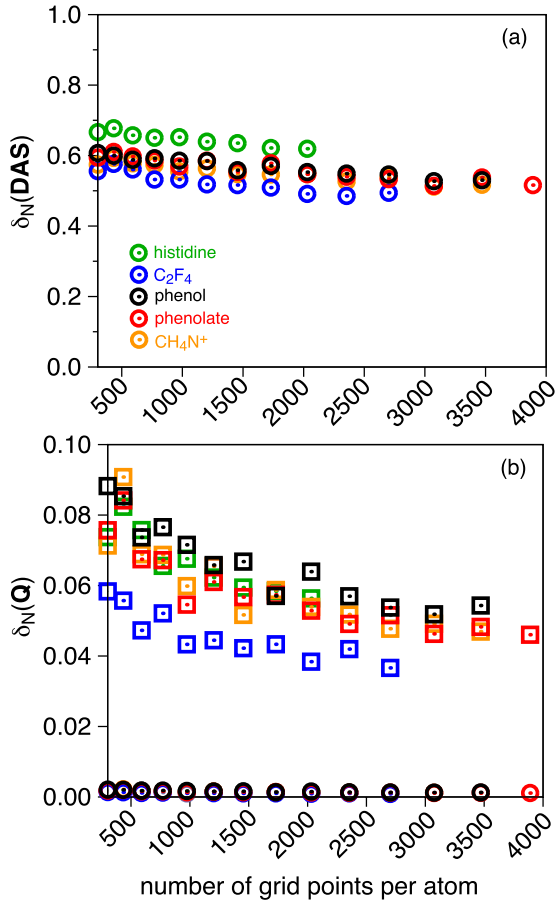

FIG. 4. Convergence of the normalized norms of the matrices (a) $\mathbf{DAS}-\mathbf{SAD}^\dagger$ and (b) $\mathbf{Q}-\mathbf{Q}^\dagger$, as a function of the number of Lebedev grid points per atomic sphere, for various test systems. In (b), the circles represent IEF-PCM and the squares are for SS(V)PE; individual colors correspond to the same molecules as in (a).

of $\|\mathbf{DAS}-\mathbf{SAD}^\dagger\|$, i.e., the denominator in Eq. (44). As a result, $\delta_N(\mathbf{DAS}) < 10^{-7}$ for each of the calculations reported in Fig. 3.

However, SWIG-PCM calculations based on the sum rule do engender positive eigenvalues of $\mathbf{Q}$ in the calculations shown in Fig. 3, for both IEF-PCM and SS(V)PE, with the latter model appearing to be more susceptible to occasionally large, positive eigenvalues. In such cases, the value of W_{pol} can differ significantly between these two models, as can be seen, for example, in Fig. 3(a) when 770 Lebedev points per atomic sphere are employed. (Some exemplary eigenvalue data can be found in the supplementary material.[65]) Thus, while the sum rule may lead to very small values of $\delta_N(\mathbf{X})$, it does not guarantee that the energy and surface charges are reasonable. Because the IEF-PCM results converge smoothly as a function of grid density, and because we value the smooth potential energy surfaces guaranteed by the SWIG discretization procedure, we choose to use SWIG in conjunction with Eq. (46).

Finally, the difference $\Delta W^{\text{MP-PP}}$ in Eq. (30) can be obtained by computing $\delta_N(\mathbf{Q})$, the normalized norm of the matrix $\mathbf{Q}-\mathbf{Q}^\dagger$. Numerical results for several different molecules (Fig. 4) demonstrate that $\delta_N(\mathbf{Q})$ is typically much smaller than $\delta_N(\mathbf{DAS})$, and we therefore anticipate based on Eq. (30) that $\Delta W^{\text{MP-PP}}$ is likely to be small. Note also that $\delta_N(\mathbf{Q})$ is an order of magnitude smaller for IEF-PCM than for SS(V)PE, suggesting a smaller difference between the Marcus and Pekar polarization energies in the IEF-PCM case.

B. Vertical excitation energies

1. Numerical results

In Table I, we compare the first-order ptSS correction, $E_i^{(1)}-W_i^{(1)}$ [Eqs. (32) and (33)] for three different PCMs, exploring both the Marcus and Pekar partitions. For C-PCM, the energy difference is numerically zero to a precision exceeding 10^{-6} eV, consistent with the formal result of a rigorously symmetric $\mathbf{Q}$ matrix. The two partitions do afford different corrections when either IEF-PCM or SS(V)PE is used, although the differences are ≤0.04 eV for SS(V)PE and <0.001 eV for IEF-PCM, for the system considered here. This is consistent with the previous observations regarding $\delta_N(\mathbf{Q})$.

Figure 5 shows the convergence of the first-order ptSS excitation energies as a function of the number of grid points. For SS(V)PE, the discrepancies between two partitions remain at ≈0.05 eV (but somewhat oscillatory) regardless of the grid density, whereas for IEF-PCM, the two partitions agree perfectly and converge quickly. These observations are in line with what we observed for $\delta_N(\mathbf{Q})$ in Sec. IV A.

The norms $\delta_N(\mathbf{DAS})$ and $\delta_N(\mathbf{Q})$ plotted in Fig. 4 are consistent with the convergence (or lack thereof) that is observed for the polarization energies in Fig. 2. In particular, the norm $\delta_N(\mathbf{Q})$ is much smaller than $\delta_N(\mathbf{DAS})$ even though $\mathbf{Q}^\dagger$ contains the ill-behaved matrix form $\mathbf{SAD}^\dagger$:

$$\mathbf{Q}^\dagger = -f_\varepsilon\left(\mathbf{I}-\frac{1}{2\pi}\mathbf{A}\mathbf{D}^\dagger\right)\left(\mathbf{S}-\frac{f_\varepsilon}{2\pi}\mathbf{X}^\dagger\right)^{-1}. \tag{47}$$

TABLE I. First-order ptSS corrections to excitation energies [Eqs. (32) and (33)]. Calculations were performed at the TDDFT level using LRC-ωPBE.

	$(E_i^{(1)}-W_i^{(1)})$/eV							
	C-PCM		SS(V)PE			IEF-PCM		
System	Marcus	Pekar	Marcus	Pekar	Difference	Marcus	Pekar	Difference
$C_2H_4\cdots CH_4N^+$[a]	−0.712 541	−0.712 541	−0.684 623	−0.644 475	−0.040 148	−0.653 487	−0.653 946	0.000 459
$C_2H_4\cdots C_2F_4$[a]	−1.146 803	−1.146 803	−1.106 555	−1.105 227	−0.001 328	−1.116 938	−1.116 084	−0.000 854
DMABN (planar)[b]	−0.124 313	−0.124 313	−0.114 169	−0.104 305	−0.009 864	−0.107 013	−0.106 883	−0.000 130
DMABN (twisted)[b]	−0.190 490	−0.190 490	−0.167 743	−0.163 528	−0.004 215	−0.165 490	−0.166 409	0.000 919

[a]In water, $\varepsilon_0 = 78.4$ and $\varepsilon_{\text{fast}} = 1.8$, with $\omega = 0.3$ bohr^{-1}.

[b]In acetonitrile, $\varepsilon_0 = 35.7$ and $\varepsilon_{\text{fast}} = 1.8$. Tuned range separation parameters are $\omega = 0.26$ and 0.28 bohr^{-1} for the planar and twisted geometries, respectively.

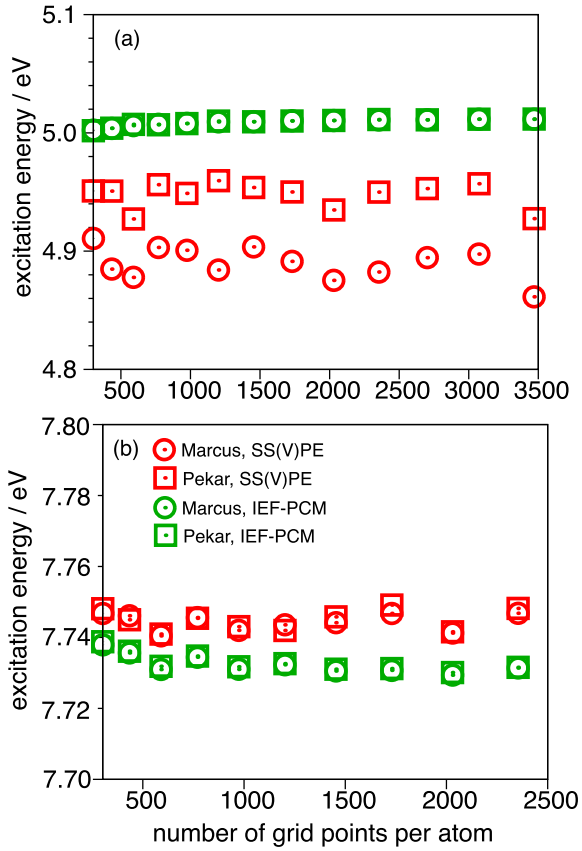

FIG. 5. Convergence of the first-order ptSS excitation energy as a function of the number of Lebedev grid points per atomic sphere for (a) $C_2H_4\cdots CH_4N^+$ and (b) $C_2H_4\cdots C_2F_4$.

The fact that $\delta_N(\mathbf{DAS}) \approx 0.6$ even for dense grids accounts for the failure of the ground-state IEF-PCM and SS(V)PE polarization energies to converge (Fig. 2), whereas the smaller values of $\delta_N(\mathbf{Q})$ presage the very small differences between Marcus and Pekar values for vertical excitation energies.

The CT systems examined in Table I were specifically selected to have relatively large ptSS solvent corrections, and as such one might reasonably question whether the very small differences between the Marcus and Pekar partitions represent some kind of numerical noise. This would be odd, given that the calculations above, e.g., in Fig. 5, use some very dense grids, but we can also address this via a systematic test on the two dimers in which we scan the two dielectric constants ε_0 and ε_{fast} across representative ranges of each. Difference between the ptSS excitation energy corrections for the two CT dimers is plotted in Fig. 6.

For IEF-PCM, the numerical difference between the two partitions increases as the ratio $\varepsilon_0/\varepsilon_{fast}$ increases, so that aqueous solvation provides the largest discrepancy. The trend is somewhat more complicated (and the differences a bit larger) for SS(V)PE, but in both cases, the trends are systematic as a function of both dielectric constants; hence, we conclude that the numerical differences observed in the calculations presented above are not artifacts. This is consistent with the formal theory in Section II. On the other hand, these calculations suggest that the practical difference between these two partitions is likely to be negligible in most cases; for realistic values $\varepsilon_{fast} < 3$, the differences observed in Fig. 6 are <0.1 eV for all values of $\varepsilon_0 \leq 80$. Differences in systems lacking in CT character are likely to be even smaller.

2. Analysis of the fast polarization response

While contributions to the energy may differ little between the two partitions, the polarization charges can be quite different, especially when the solvent is polar. In that case, very different fast and slow charges are obtained in the ground state, whereas the fast charges obtained in the excited state are more comparable. In the case of aqueous $C_2H_4\cdots CH_4N^+$, for example, the total absolute fast charge in the first excited state is $\approx 0.62e$ in the Marcus case and $\approx 0.52e$ in the Pekar case (see Fig. 7). The ground-state charge is $\approx 0.012e$ in the Marcus case; hence, the change in the fast charges upon excitation is considerable. Since only the fast solvent degrees of freedom can follow the density change in the solute, it is reasonable that there is significant fast charge contribution to the total surface charge in the excited state, given the large change in solute density upon excited-state electron transfer from C_2H_4 to CH_4N^+.

Figure 7(b) illustrates the fast excited-state charge distributions that are obtained in the Marcus and Pekar partitions for the $C_2H_4 \rightarrow CH_4N^+$ charge-transfer excitation. From Eq. (21), one expects that the fast charge distribution in the Pekar case is essentially the image charge of the solute's excited-state charge distribution, and this is clear from Fig. 7(b) when one compares the Pekar fast charge distribution and the corresponding electrostatic potential to atomic charges derived from natural population analysis,[68] as applied to the excited-state electron density. Within the Marcus partition, however, the CH_4N^+ moiety exhibits a more pronounced positive charge, and the fast charge on C_2H_4 is correspondingly less negative, an effect that arises from the remaining negative surface charges in the ground state. This ground-state fast charge is essentially absent in the Marcus partition.

The mutual influence of fast and slow charges gives rise to different physical pictures of non-equilibrium polarization. Whereas the fast charge in the Pekar case is image-like, the fast charge in the Marcus case can be viewed as the solvent polarization due to the density difference between the ground and excited states. [Recall that the difference $\Delta W_i^{\text{MP-PP}}$ between the SS polarization energies in the two partitions is determined by the electrostatic potential arising from the density difference, Eq. (28).]

3. Comparison to experimental solvent shift

Intuitively, the electrostatic interactions in a non-equilibrium process should be dictated by the optical dielectric constant. Since there is relatively little variation in ε_{opt} from one solvent to the next,[34] we anticipate that the solvent corrections should not vary by much. Results for the 2 A_1 state of nitrobenzene (Table II) indeed indicate that the ptSS corrections ($E^{(1),\text{ptSS}}$) change little from one solvent to the next. We also calculated the ptLR correction ($E^{(1),\text{ptLR}}$) to this state and find it to be nearly identical to the ptSS result. As discussed in Section II, the SS method that we have implemented neglects the dynamical correlations between

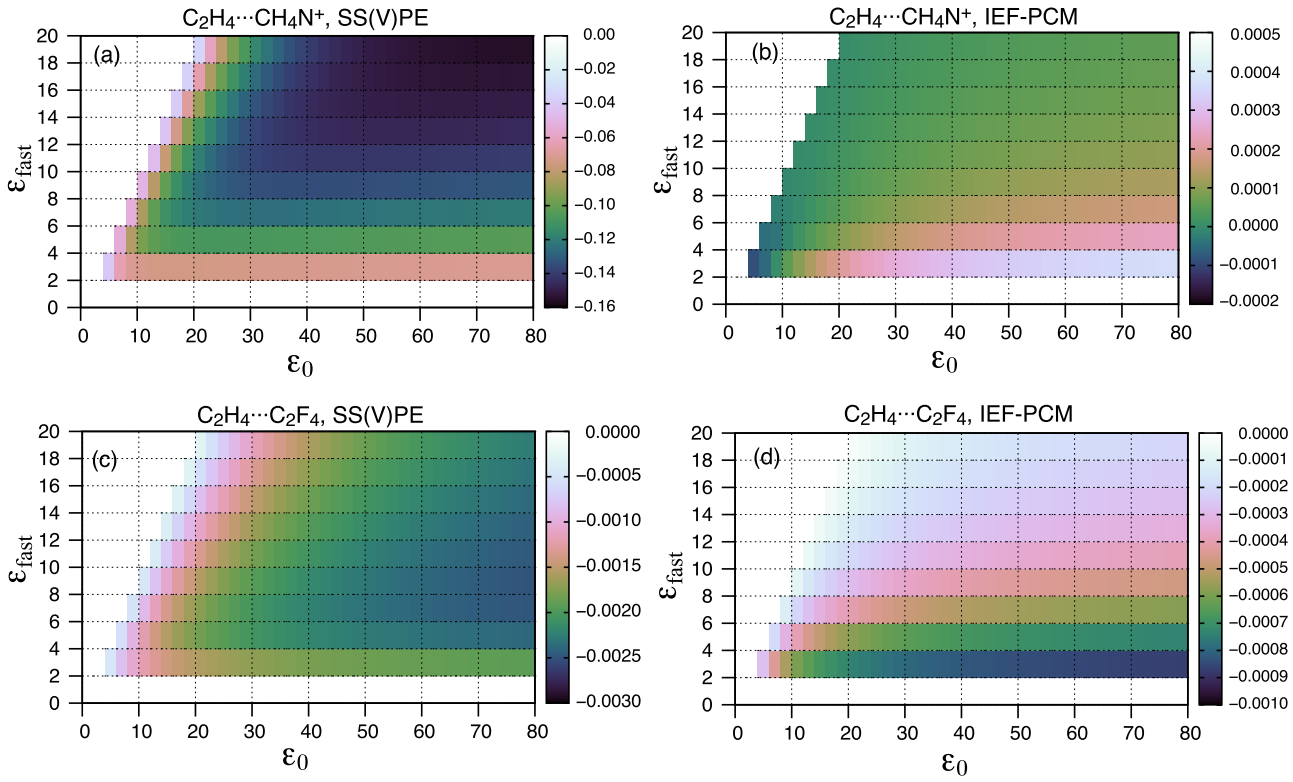

FIG. 6. Differences (in eV) in first-order ptSS excitation energy corrections between the Marcus and Pekar partitions, as a function of ε_0 and $\varepsilon_{\text{fast}}$, for $C_2H_4\cdots CH_4N^+$ and $C_2H_4\cdots C_2F_4$.

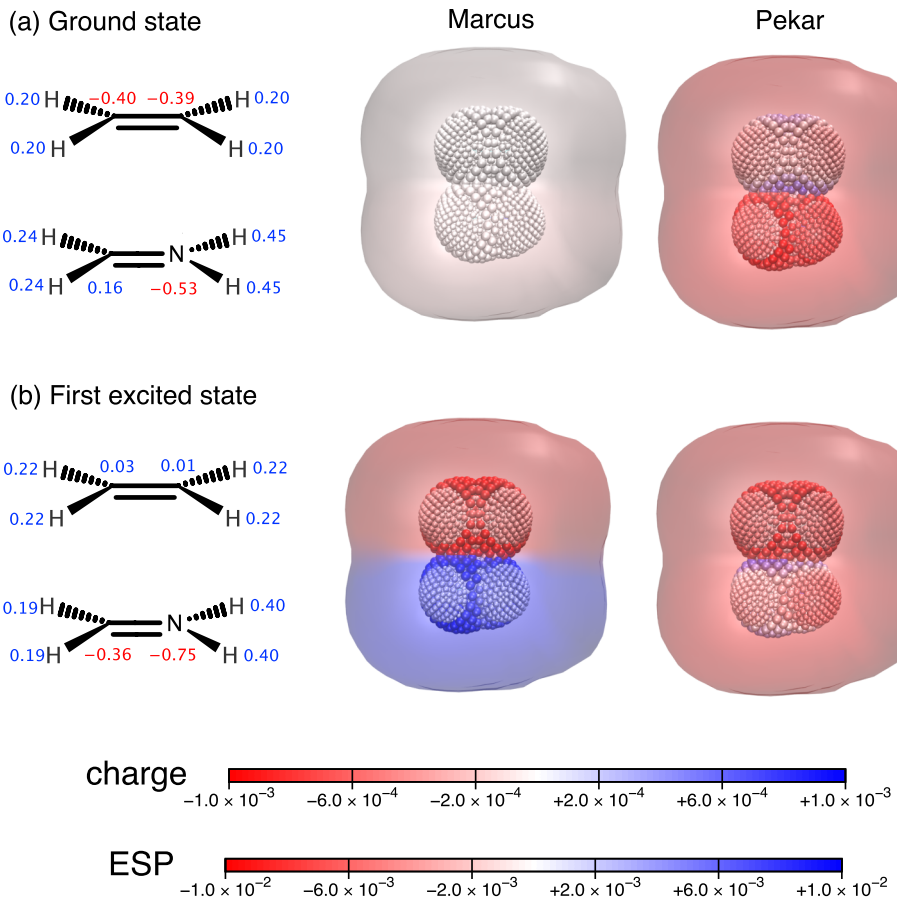

FIG. 7. Electrostatics and fast solvent polarization for (a) the equilibrium ground state and (b) the non-equilibrium excited state of $C_2H_4\cdots CH_4N^+$. The molecular structure diagrams on the left provide the ground- and excited-state atomic charges obtained from natural population analysis.[68] The center panels illustrate the fast polarization charges obtained from the Marcus partition, along with the electrostatic potential that they generate, while the panels on the right illustrate the same quantities according to the Pekar partition.

TABLE II. First-order ptSS and ptLR corrections to excitation energies and solvent shifts for the 2 A_1 ($\pi\pi^*$) excited state of nitrobenzene in various solvents. Calculations were performed using TDDFT at the LRC-ωPBE/cc-pVDZ/C-PCM level, with $\omega = 0.29$ bohr^{-1}.

	Gas phase	Hexane	Cyclo-hexane	Diethyl ether	Acetonitrile
$\Delta E^{(0)}$	5.477	5.383	5.373	5.300	5.225
$E^{(1),\mathrm{ptSS}}$		−0.0711	−0.0771	−0.0708	−0.0708
$E^{(1),\mathrm{ptLR}}$		−0.0739	−0.0801	−0.0736	−0.0748
Solvent shift[a]		−0.218	−0.239	−0.300	−0.376
Expt. shift[b]		−0.226			−0.414
$\varepsilon_{\mathrm{opt}}$		1.88	2.02	1.83	1.8
ε_0		1.89	2.03	4.32	35.7

[a]Computed using Eq. (48).
[b]From Ref. 38.

solute and solvent; however, this correlation is partially recovered by the LR correction.[45,46] [See the discussion surrounding Eq. (36).] This might suggest that the combination of ptSS and ptLR solvation corrections could reproduce experimental solvent shifts, an approach that corresponds to a solvent shift computed as

$$\text{shift} = \Delta E^{(0)} + \Delta E^{\mathrm{ptSS}} + \Delta E^{\mathrm{ptLR}} - \Delta E^{(0)}_{\mathrm{gas}}. \qquad (48)$$

In the nitrobenzene example of Table II, the ptLR and ptSS energies are both comparable and complementary, as suggested in Ref. 21. The calculated solvent shifts (in hexane and acetonitrile) are very consistent with experimental values from Ref. 38.

It has been suggested that the difference between LR and SS results lies in a flaw in the LR formalism that renders it incapable of describing a non-stationary state, in which the system cannot be represented as a single Hartree product of a solute state and a solvent state.[45,46] At the same time, it has long been suggested that the LR model captures dynamical correlation effects, i.e., dispersion.[46,69,70] As such, a combination of the ptSS and ptLR corrections may be viewed as an empirical fitting to the experimental data. Other scaling variants are possible. In our recent work,[38] the most accurate combinations are provided and discussed for ADC and TDDFT based on a set of experimental benchmark data.

C. Vertical ionization energies

Finally, we consider a vertical ionization process, and VIEs for aqueous phenol and phenolate are reported in Table III. Once again, the numerical calculations confirm that there is no difference whatsoever between the Marcus and Pekar energetics when C-PCM is used. Differences in the VIEs computed using IEF-PCM versus SS(V)PE are 0.002–0.005 eV, except for SS(V)PE as applied to phenolate, where the difference is 0.131 eV. As observed above and in previous work,[7] this is consistent with observations concerning $\delta_{\mathrm{N}}(\mathbf{Q})$ and reflects the larger difference between symmetrized and unsymmetrized $\mathbf{K}$ matrices for charged systems. In the IEF-PCM calculations, the self-consistent field energies of the ionized species (phenol cation and phenolate radical) are numerically identical in the two partitions ($E^{\mathrm{SS}}_{\mathrm{ionic}}$ = −306.883 746 51 and −306.565 403 53 hartree, respectively), and thus, the small differences in Table III reflect differences in the polarization energy.

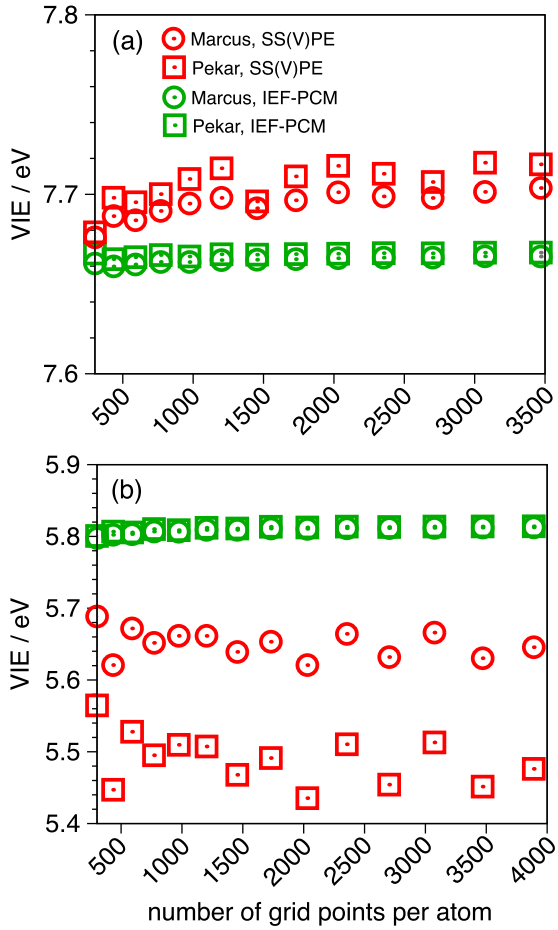

FIG. 8. Convergence of the VIEs as a function of the number of Lebedev grid points per atomic sphere for (a) phenol and (b) phenolate.

Figure 8 shows how the VIEs converge as a function of the discretization grid. Consistent with results for vertical

TABLE III. VIEs for aqueous phenol and phenolate, computed at the SS-DFT/LRC-ωPBE level with optimally tuned values $\omega = 0.30$ bohr^{-1} (phenol) and $\omega = 0.27$ bohr^{-1} (phenolate).

	Vertical ionization energy/eV							
	C-PCM		SS(V)PE			IEF-PCM		
Solute	Marcus	Pekar	Marcus	Pekar	Difference	Marcus	Pekar	Difference
Phenol	7.656 817	7.656 817	7.676 073	7.678 798	−0.002 725	7.661 498	7.666 971	−0.005 473
Phenolate	5.794 856	5.794 856	5.688 647	5.564 663	0.123 984	5.797 936	5.800 617	−0.002 681

TABLE IV. VIEs for aqueous phenol and phenolate, computed using C-PCM with different empirical scaling functions, $\widetilde{f}_\varepsilon(x)$ [Eq. (50)]. Note that C-PCM as implemented by Barone and Cossi[6] uses $x = 0$, whereas the conductor-like screening model of Klamt and Schüürmann[5] uses $x = 0.5$. The "mixed" scheme suggested in Ref. 71 uses $x = 0.5$ for neutral solutes and $x = 0$ for ionic ones. Calculations were performed at the SS-DFT/LRC-ωPBE level with optimally tuned values $\omega = 0.30$ bohr^{-1} (phenol) and $\omega = 0.27$ bohr^{-1} (phenolate).

	Vertical ionization energy/eV						
	$x = 0$		$x = 0.5$		Mixed		
Solute	Marcus	Pekar	Marcus	Pekar	Marcus	Pekar	Difference
Phenol	7.656 817	7.656 817	7.876 567	7.876 567	7.656 455	7.628 749	0.027 706
Phenolate	5.794 856	5.794 856	5.983 149	5.983 149	6.002 801	5.834 784	0.168 017

excitation energies, we find almost no difference between the Marcus and Pekar values in the case of IEF-PCM, whereas there is some numerical discrepancy in the case of SS(V)PE. In the latter case, the magnitude of the difference is not terribly sensitive to the discretization grid and remains at ≈0.01 eV for phenol and ≈0.15 eV for phenolate, although the difference does inherit some oscillations as the grid density increases.

Recently, Klamt *et al.*[71] have demonstrated excellent agreement between solvation energies computed using IEF-PCM/SS(V)PE and those obtained using the much simpler C-PCM approach, if the surface charges in the latter are scaled appropriately. The C-PCM equation, which should be compared to Eq. (39), is

$$\mathbf{Sq} = \widetilde{f}_\varepsilon(x)\mathbf{v} \tag{49}$$

with

$$\widetilde{f}_\varepsilon(x) = \frac{\varepsilon - 1}{\varepsilon + x}. \tag{50}$$

The values $x = 1/2$ for neutral solutes and $x = 0$ for ions are suggested.[71] [Note that IEF-PCM/SS(V)PE uses $x = 1$ in the factor of f_ε that appears in the definition of $\mathbf{R}_\varepsilon$, Eq. (40).] Table IV presents the C-PCM VIEs for aqueous phenol and phenolate, using various values for x. When a common value of x is used for both charge states, then the Marcus and Pekar approaches to computing the VIE are formally and numerically equivalent, just as in the case of vertical excitation energies. When different value of x is used for the neutral species and the ion, however (as suggested in Ref. 71), then the two factors of $\hat{Q}_{\varepsilon_{\text{fast}}}$ in Eq. (23) are not longer the same, and the Marcus and Pekar partitions differ. Unlike the discrepancies introduced by the choice of **DAS** versus **SAD**†, which are in some sense artifacts of the discretization process, in this case, the operators $\hat{Q}_{\varepsilon_{\text{fast}}}$ really are different, even at the level of integral equations. As such, it is perhaps not surprising that the differences between Marcus and Pekar results are somewhat larger than what is observed above, as large as 0.17 eV for phenolate.

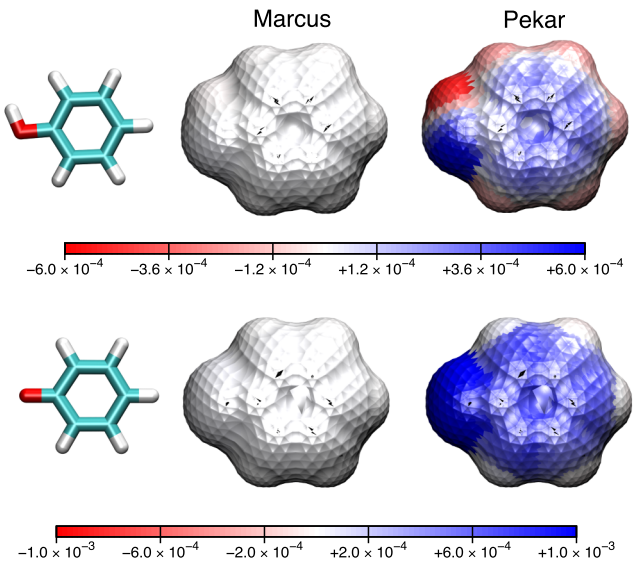

FIG. 9. Fast solvent polarization charges in the equilibrium ground state of aqueous phenol and aqueous phenolate. In each figure, the middle (mostly featureless) panel depicts the fast charges within the Marcus partition, and the rightmost figure depicts the fast charges within the Pekar partition. Both the Marcus and Pekar charges are plotted on a common scale.

With the exception of this somewhat special case, however, differences between the Marcus and Pekar partitions appear to be quite small, even in systems specifically selected to exhibit large solvent corrections. That said, one should keep in mind that the partition between fast and slow charges in the ground state is very different in these two schemes, even if they afford nearly identical energetics. This was seen already in the CT excitation of $C_2H_4 \cdots CH_4N^+$ (Fig. 7) but is also apparent by comparing Marcus and Pekar fast polarization charges for vertical ionization (Fig. 9). In a highly polar solvent such as water, the fast charge obtained within the Marcus partition is negligible as compared to that in the Pekar partition, as we have already discussed in the context of Eq. (10). Using the sum of the absolute values of the discretized surface point charges as a measure of the total surface charge, we obtain a total fast charge of ≈0.01e for phenolate in the Marcus case, and ≈0.45e in the Pekar case.

V. CONCLUSION

We have examined the partition dependence of the state-specific, non-equilibrium solvation method within the framework of quantum-mechanical PCMs. At the level of integral equations, the non-equilibrium corrections to vertical excitation and ionization energies are formally equivalent when the "fast" and "slow" solvent responses are partitioned in the Marcus way[27,28] or according to the Pekar scheme.[29] Discretization does not preserve this equivalence, however, except in the special case of the conductor-like PCMs. This

arises due to loss of certain symmetries when the PCM integral equations are discretized (as has been discussed previously in the context of equilibrium solvation[7]), along with the loss of a sum rule [Eq. (45)] when the surface discretization is rendered smooth via a switching function.

Numerical calculations indicate that the discrepancies in vertical ionization energies are $\lesssim$0.1 eV between the two partitions, except in one particular case where C-PCM is used with different scaling factors for neutral versus ionic solutes, as was advocated in a recent study.[71] Discrepancies in vertical excitation energies are smaller still. Such differences are considerably smaller than the intrinsic error in the continuum approximation itself, so it appears that, in practice, the Marcus and Pekar partitions can be used interchangeably. However, caution should be exercised in placing any interpretative significance in the values of the fast polarization charges themselves, which are highly partition-dependent (especially in high-dielectric solvents). This is an inherent feature, not an artifact of discretization.

ACKNOWLEDGMENTS

Work by Z.-Q.Y. and J.M.H. was supported by the U.S. National Science Foundation, under Grant No. CHE-1300603, and calculations were performed at the Ohio Supercomputer Center under Award No. PAA-0003.[72] J.M.H. is a Camille Dreyfus Teacher-Scholar.

[1]J. Tomasi, B. Mennucci, and R. Cammi, Chem. Rev. **105**, 2999 (2005).
[2]A. Klamt, WIREs Comput. Mol. Sci. **1**, 699 (2011).
[3]B. Mennucci, WIREs Comput. Mol. Sci. **2**, 386 (2012).
[4]J. M. Herbert and A. W. Lange, "Polarizable continuum models for (bio)molecular electrostatics: Basic theory and recent developments for macromolecules and simulations," in *Many-Body Effects and Electrostatics in Biomolecules*, edited by Q. Cui, P. Ren, and M. Meuwly (Pan Stanford, 2015), Chap. 1, pp. 1–54.
[5]A. Klamt and G. Schüürmann, J. Chem. Soc., Perkin Trans. 2 **1993**, 799.
[6]V. Barone and M. Cossi, J. Phys. Chem. A **102**, 1995 (1998).
[7]A. W. Lange and J. M. Herbert, Chem. Phys. Lett. **509**, 77 (2011).
[8]J. Tomasi, B. Mennucci, and E. Cancès, J. Mol. Struct.: THEOCHEM **464**, 211 (1999).
[9]E. Cancès and B. Mennucci, J. Chem. Phys. **114**, 4744 (2001).
[10]D. M. Chipman, J. Chem. Phys. **112**, 5558 (2000).
[11]D. M. Chipman, Theor. Chem. Acc. **107**, 80 (2002).
[12]C. J. Cramer and D. G. Truhlar, Acc. Chem. Res. **41**, 760 (2008).
[13]A. Klamt, B. Mennucci, J. Tomasi, V. Barone, C. Curutchet, M. Orozco, and F. J. Luque, Acc. Chem. Res. **42**, 489 (2009).
[14]A. Pomogaeva and D. M. Chipman, J. Chem. Theory Comput. **10**, 211 (2014).
[15]A. Pomogaeva and D. M. Chipman, J. Phys. Chem. A **119**, 5173 (2015).
[16]R. Cammi and B. Mennucci, J. Chem. Phys. **110**, 9877 (1999).
[17]M. Cossi and V. Barone, J. Chem. Phys. **115**, 4708 (2001).
[18]J. Tomasi and M. Persico, Chem. Rev. **94**, 2027 (1994).
[19]R. Cammi and J. Tomasi, Int. J. Quantum Chem., Symp. **29**, 465 (1995).
[20]M. Cossi and V. Barone, J. Phys. Chem. A **104**, 10614 (2000).
[21]R. Improta, V. Barone, G. Scalmani, and M. J. Frisch, J. Chem. Phys. **125**, 054103 (2006).
[22]R. Cammi, Int. J. Quantum Chem. **110**, 3040 (2010).
[23]R. Cammi, R. Fukuda, M. Ehara, and H. Nakatsuji, J. Chem. Phys. **133**, 024104 (2010).
[24]R. Fukuda, M. Ehara, H. Nakatsuji, and R. Cammi, J. Chem. Phys. **134**, 104109 (2011).
[25]M. Caricato, J. Chem. Theory Comput. **8**, 4494 (2012).
[26]M. Caricato, J. Chem. Theory Comput. **8**, 5081 (2012).
[27]R. A. Marcus, J. Chem. Phys. **24**, 966 (1956).
[28]R. A. Marcus, J. Chem. Phys. **24**, 979 (1956).
[29]S. I. Pekar, Research in electron theory of crystals, Technical Report No. AEC–tr–5575, U.S. Atomic Energy Commission, Division of Technical Information, 1963.
[30]J. E. Brady and P. W. Carr, J. Phys. Chem. **89**, 5759 (1985).
[31]A. Klamt, J. Phys. Chem. **100**, 3349 (1996).
[32]C. J. F. Böttcher and P. Bordewijk, *Theory of Electric Polarization*, 2nd ed. (Elsevier, New York, 1973), Vol. II.
[33]N. S. Bayliss and R. G. McRae, J. Phys. Chem. **58**, 1006 (1954).
[34]See http://www.stenutz.eu/chem/solv23.php for a list of indices of refraction for common solvents.
[35]M. Cossi and V. Barone, J. Chem. Phys. **112**, 2427 (2000).
[36]M. A. Aguilar, J. Phys. Chem. A **105**, 10393 (2001).
[37]A. V. Marenich, C. J. Cramer, D. G. Truhlar, C. A. Guido, B. Mennucci, G. Scalmani, and M. J. Frisch, Chem. Sci. **2**, 2143 (2011).
[38]J.-M. Mewes, Z.-Q. You, M. Wormit, T. Kriesche, J. M. Herbert, and A. Dreuw, J. Phys. Chem. A **119**, 5446 (2015).
[39]L. D. Jacobson, C. F. Williams, and J. M. Herbert, J. Chem. Phys. **130**, 124115 (2009).
[40]M. A. Aguilar, F. J. Olivares del Valle, and J. Tomasi, J. Chem. Phys. **98**, 7375 (1993).
[41]D. M. Chipman, J. Chem. Phys. **131**, 014103 (2009).
[42]F. Lipparini, G. Scalmani, B. Mennucci, E. Cancès, M. Caricato, and M. J. Frisch, J. Chem. Phys. **133**, 014106 (2010).
[43]A. W. Lange and J. M. Herbert, J. Chem. Phys. **133**, 244111 (2010).
[44]L. D. Jacobson and J. M. Herbert, J. Chem. Theory Comput. **7**, 2085 (2011).
[45]R. Cammi, S. Corni, B. Mennucci, and J. Tomasi, J. Chem. Phys. **122**, 104513 (2005).
[46]S. Corni, R. Cammi, B. Mennucci, and J. Tomasi, J. Chem. Phys. **123**, 134512 (2005).
[47]M. Caricato, B. Mennucci, J. Tomasi, F. Ingrosso, R. Cammi, S. Corni, and G. Scalmani, J. Chem. Phys. **124**, 124520 (2006).
[48]B. Lunkenheimer and A. Köhn, J. Chem. Theory Comput. **9**, 977 (2013).
[49]F. Furche and R. Ahlrichs, J. Chem. Phys. **117**, 7433 (2002).
[50]A. Dreuw and M. Wormit, WIREs Comput. Mol. Sci. **5**, 82 (2015).
[51]F. Plasser, M. Wormit, and A. Dreuw, J. Chem. Phys. **140**, 024106 (2014).
[52]F. Plasser, S. A. Bäppler, M. Wormit, and A. Dreuw, J. Chem. Phys. **141**, 024107 (2014).
[53]N. Ghoneim and P. Suppan, Pure Appl. Chem. **65**, 1739 (1993).
[54]M. Hashimoto and H. Hamaguchi, J. Phys. Chem. **99**, 7875 (1995).
[55]Z. R. Grabowski, K. Rotkiewicz, and W. Rettig, Chem. Rev. **103**, 3899 (2003).
[56]D. Ghosh, A. Roy, R. Seidel, B. Winter, S. Bradforth, and A. I. Krylov, J. Phys. Chem. B **116**, 7269 (2012).
[57]T. M. Henderson, B. G. Janesko, and G. E. Scuseria, J. Chem. Phys. **128**, 194105 (2008).
[58]M. A. Rohrdanz, K. M. Martins, and J. M. Herbert, J. Chem. Phys. **130**, 054112 (2009).
[59]R. Baer, E. Livshits, and U. Salzner, Annu. Rev. Phys. Chem. **61**, 85 (2010).
[60]T. Stein, L. Kronik, and R. Baer, J. Am. Chem. Soc. **131**, 2818 (2009).
[61]T. Minami, M. Nakano, and F. Castet, J. Phys. Chem. Lett. **2**, 1725 (2011).
[62]D. M. Chipman and M. Dupuis, Theor. Chem. Acc. **107**, 90 (2002).
[63]Y. Shao, Z. Gan, E. Epifanovsky, A. T. B. Gilbert, M. Wormit, J. Kussmann, A. W. Lange, A. Behn, J. Deng, X. Feng, D. Ghosh, M. Goldey, P. R. Horn, L. D. Jacobson, I. Kaliman, R. Z. Khaliullin, T. Kús, A. Landau, J. Liu, E. I. Proynov, Y. M. Rhee, R. M. Richard, M. A. Rohrdanz, R. P. Steele, E. J. Sundstrom, H. L. Woodcock III, P. M. Zimmerman, D. Zuev, B. Albrecht, E. Alguire, B. Austin, G. J. O. Beran, Y. A. Bernard, E. Berquist, K. Brandhorst, K. B. Bravaya, S. T. Brown, D. Casanova, C.-M. Chang, Y. Chen, S. H. Chien, K. D. Closser, D. L. Crittenden, M. Diedenhofen, R. A. DiStasio, Jr., H. Dop, A. D. Dutoi, R. G. Edgar, S. Fatehi, L. Fusti-Molnar, A. Ghysels, A. Golubeva-Zadorozhnaya, J. Gomes, M. W. D. Hanson-Heine, P. H. P. Harbach, A. W. Hauser, E. G. Hohenstein, Z. C. Holden, T.-C. Jagau, H. Ji, B. Kaduk, K. Khistyaev, J. Kim, J. Kim, R. A. King, P. Klunzinger, D. Kosenkov, T. Kowalczyk, C. M. Krauter, K. U. Lao, A. Laurent, K. V. Lawler, S. V. Levchenko, C. Y. Lin, F. Liu, E. Livshits, R. C. Lochan, A. Luenser, P. Manohar, S. F. Manzer, S.-P. Mao, N. Mardirossian, A. V. Marenich, S. A. Maurer, N. J. Mayhall, C. M. Oana, R. Olivares-Amaya, D. P. O'Neill, J. A. Parkhill, T. M. Perrine, R. Peverati, P. A. Pieniazek, A. Prociuk, D. R. Rehn, E. Rosta, N. J. Russ, N. Sergueev, S. M. Sharada, S. Sharmaa, D. W. Small, A. Sodt, T. Stein, D. Stück, Y.-C. Su, A. J. W. Thom, T. Tsuchimochi, L. Vogt, O. Vydrov, T. Wang, M. A. Watson, J. Wenzel, A. White, C. F. Williams, V. Vanovschi, S. Yeganeh, S. R. Yost, Z.-Q. You, I. Y. Zhang, X. Zhang, Y. Zhou, B. R. Brooks, G. K. L. Chan, D. M. Chipman, C. J. Cramer, W. A. Goddard III, M. S. Gordon, W. J. Hehre, A. Klamt, H. F. Schaefer III, M. W.

Schmidt, C. D. Sherrill, D. G. Truhlar, A. Warshel, X. Xua, A. Aspuru-Guzik, R. Baer, A. T. Bell, N. A. Besley, J.-D. Chai, A. Dreuw, B. D. Dunietz, T. R. Furlani, S. R. Gwaltney, C.-P. Hsu, Y. Jung, J. Kong, D. S. Lambrecht, W. Liang, C. Ochsenfeld, V. A. Rassolov, L. V. Slipchenko, J. E. Subotnik, T. Van Voorhis, J. M. Herbert, A. I. Krylov, P. M. W. Gill, and M. Head-Gordon, Mol. Phys. **113**, 184 (2015).
[64]A. W. Lange and J. M. Herbert, J. Phys. Chem. Lett. **1**, 556 (2010).
[65]See supplementary material at http://dx.doi.org/10.1063/1.4936357 for additional data comparing the fixed point charge and SWIG discretization schemes.
[66]E. O. Purisima and S. H. Nilar, J. Comput. Chem. **16**, 681 (1995).
[67]B. Mennucci, E. Cancès, and J. Tomasi, J. Phys. Chem. B **101**, 10506 (1997).
[68]A. E. Reed, R. B. Weinstock, and F. Weinhold, J. Chem. Phys. **83**, 735 (1985).
[69]E. G. McRae, J. Phys. Chem. **61**, 562 (1957).
[70]N. Rösch and M. C. Zerner, J. Phys. Chem. **98**, 5817 (1994).
[71]A. Klamt, C. Moya, and J. Palomar, J. Chem. Theory Comput. **11**, 4220 (2015).
[72]Ohio Supercomputer Center, http://osc.edu/ark:/19495/f5s1ph73 (accessed November 3, 2015).